Electronic Supplementary Information (ESI) for:

The Raman spectrum of isolated water clusters

Katharina E. Otto, Zhifeng Xue, Philipp Zielke, and Martin A. Suhm

Institut für Physikalische Chemie, Georg-August-Universität Göttingen, Tammannstraße 6, 37077 Göttingen, Germany

SPECTRAL DETAILS

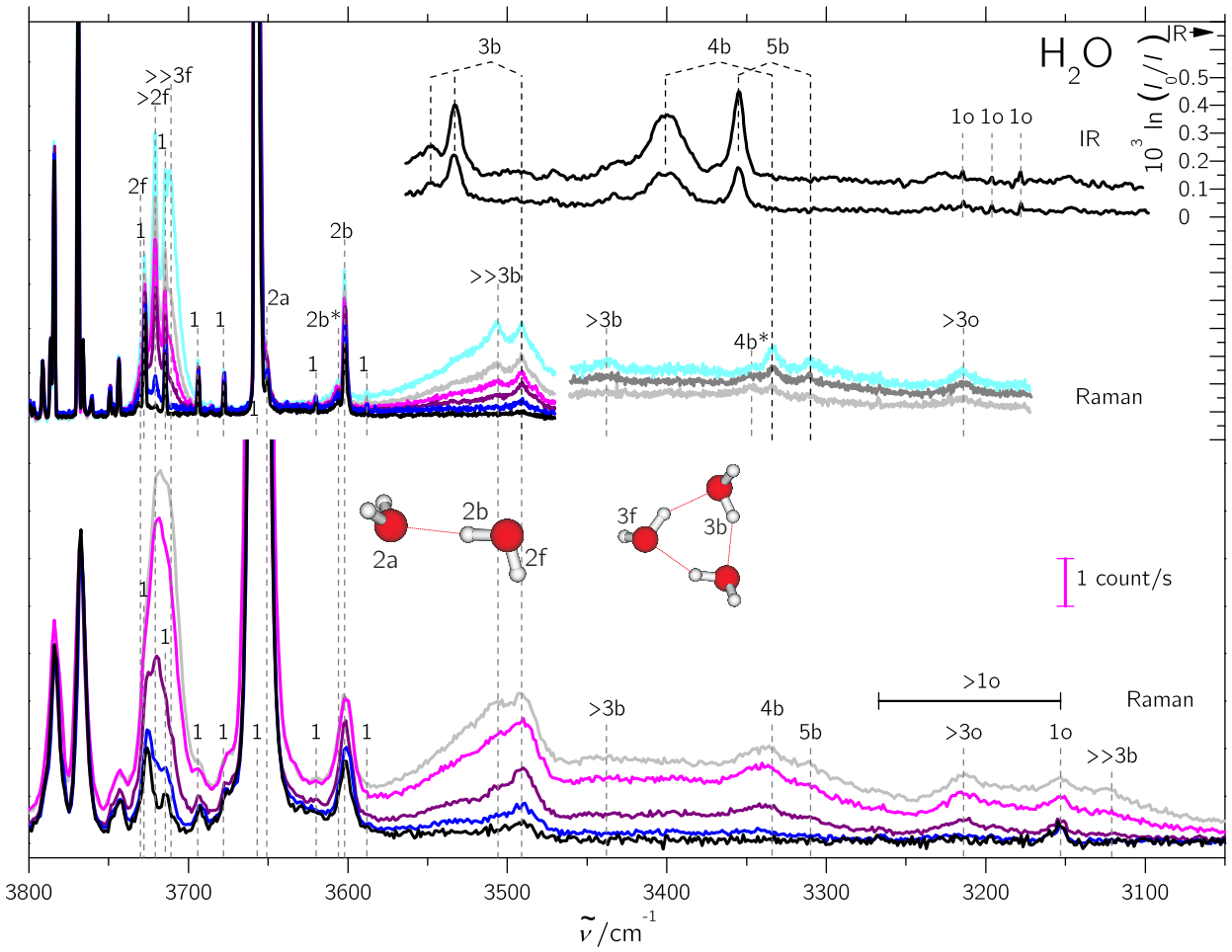

Fig. S 1. H_2O clusters: Raman and IR[1] spectra of H_2O expansions. Raman spectra were scaled to the same monomer intensity in the respective blocks. The labels denote: 1,2,3,4,5 = number of molecules in the cluster, b = bound, f = free, a = acceptor, o = bending overtone, * = hot band.

Lower part: Raman spectra of He-expansions seeded with water recorded with a 0.5 m monochromator (McPherson model 205f, grating: 600 #/mm). Detailed information on the measurement conditions, such as nozzle temperature ϑ_n, saturator temperature ϑ_s and stagnation pressure p_s can be found in table S I.

Upper part: Similar conditions but recorded with a 1 m monochromator (McPherson Model 2051, grating 1200 #/mm). Detailed information, also on the IR spectra, see tab. S I.

#	colour/trace	ϑ_s/°C	ϑ_n/°C	p_s/bar	carrier gas	scaling factor	acquisition time	nozzle size	nozzle distance
		Lower part, from bottom to top							
H1	black	10	120	0.7	100% He	2.13	12×300 s	4×0.15 mm^2	2 mm
H2	blue	18	120	0.7	100% He	1.27	12×300 s	4×0.15 mm^2	2 mm
H3	purple	22	120	1.0	100% He	1.12	12×300 s	4×0.15 mm^2	2 mm
H4	pink	22	80	1.0	100% He	1.00	12×300 s	4×0.15 mm^2	2 mm
H5	grey	22	25	1.0	100% He	1.00	12×300 s	4×0.15 mm^2	2 mm
		Upper left, from bottom to top							
H6	black	10	120	0.7	100% He	2.00	18×200 s	4×0.15 mm^2	2 mm
H7	blue	18	120	0.7	100% He	1.34	18×100 s	4×0.15 mm^2	2 mm
H8	purple	18	120	1.0	100% He	1.01	18×100 s	4×0.15 mm^2	2 mm
H9	pink	18	80	1.0	100% He	1.00	18×100 s	4×0.15 mm^2	2 mm
H10	grey	18	25	1.0	100% He	1.05	18×100 s	4×0.15 mm^2	2 mm
H11	light blue	18	25	0.7	20% Ar in He	1.20	12×300 s	4×0.15 mm^2	2 mm
		Upper right from ref. 2, from bottom to top							
H12	grey	22	25	1.2	100% He	1.90	12×300 s	8×0.05 mm^2	2 mm
H13	dark grey	22	25	1.2	20% Ne in He	2.00	12×300 s	8×0.05 mm^2	2 mm
H14	light blue	22	25	1.2	20% Ar in He	2.80	12×300 s	8×0.05 mm^2	2 mm

	Upper right IR-spectra from ref. 1, from bottom to top			
trace	concentration	p_s/bar	carrier gas	scans
upper	0.2%	1.6	He	400
lower	0.7%	1.0	He	361

Tab. S I. Measurement conditions for spectra depicted in fig. S 1. The count rate denoted in fig. S 1 refers to spectra #H4 and #H9.

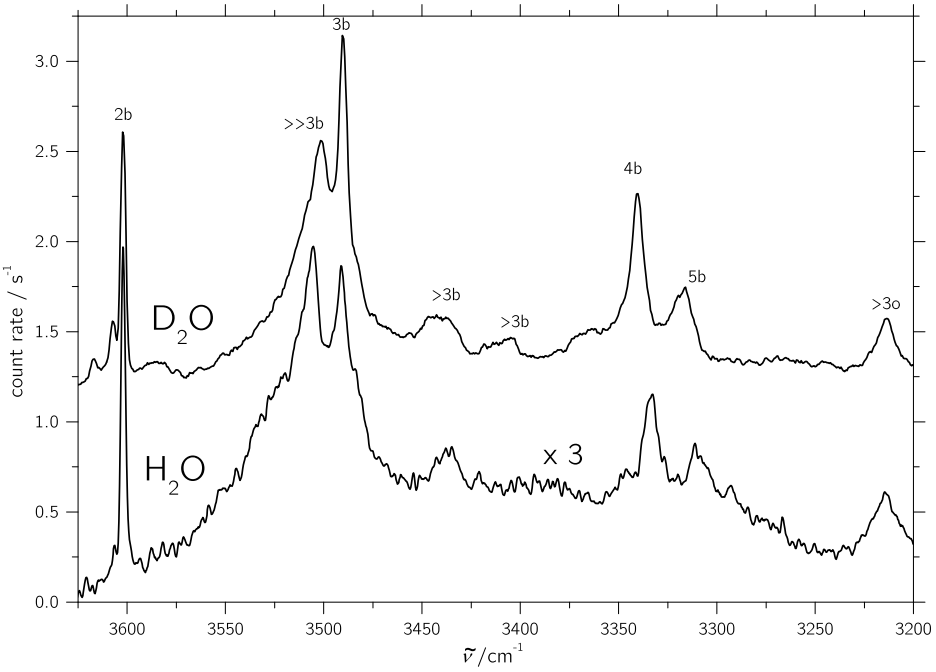

Fig. S 2. Correspondence between Raman jet spectra of H_2O and D_2O clusters scaled to similar intensity. Wavenumbers of D_2O spectra have been stretched by 1.498 and then 342.4 cm^{-1} was subtracted. The substances were expanded in He/Ar rare gas mixtures (spectra #H14 in fig. S1 and #D12 in fig. S3.)

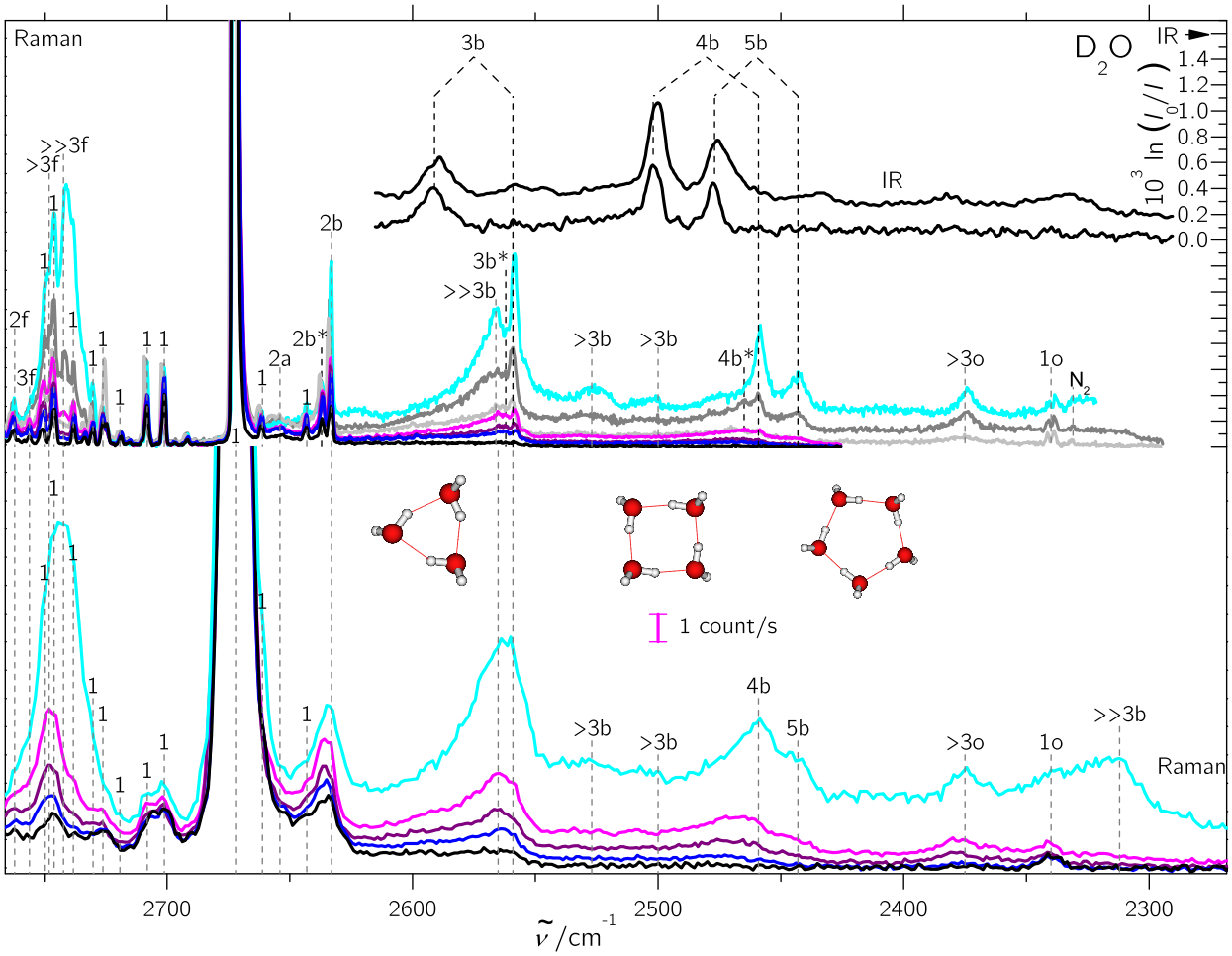

Fig. S 3. D_2O clusters: Raman and IR[1] spectra of D_2O expansions. Raman spectra were scaled to the same monomer intensity in the respective blocks. The labels are explained in fig. S1.

Lower part: Raman spectra of He- or He/Ar-expansions respectively seeded with water recorded with a 0.5 m monochromator (McPherson model 205f, grating: 600 #/mm). Detailed information on the measurement conditions, such as nozzle temperature ϑ_n, saturator temperature ϑ_s and stagnation pressure p_s can be found in table S II.

Upper part: Similar conditions but recorded with a 1 m monochromator (McPherson Model 2051, grating 1200 #/mm). Detailed information, also on the IR spectra, see tab. S II.

#	colour	ϑ_s/°C	ϑ_n/°C	p_s/bar	carrier gas	scaling factor	acquisition time	nozzle size	nozzle distance
		Lower part, from bottom to top							
D1	black	10	120	0.7	100% He	1.72	12×300 s	4×0.15 mm^2	2 mm
D2	blue	18	120	0.7	100% He	1.62	12×300 s	4×0.15 mm^2	2 mm
D3	purple	18	120	0.7	100% He	1.12	12×300 s	4×0.15 mm^2	2 mm
D4	pink	18	80	0.7	100% He	1.00	12×300 s	4×0.15 mm^2	2 mm
D5	light blue	18	25	0.7	20% Ar in He	1.21	12×300 s	4×0.15 mm^2	2 mm
		Upper part, from bottom to top							
D6	black	10	120	0.7	100% He	1.59	36×100 s	4×0.15 mm^2	2 mm
D7	blue	18	120	0.7	100% He	1.35	18×100 s	4×0.15 mm^2	2 mm
D8	purple	18	120	1.0	100% He	1.30	18×100 s	4×0.15 mm^2	2 mm
D9	pink	18	80	1.0	100% He	1.00	18×100 s	4×0.15 mm^2	2 mm
		Upper part Raman spectra from ref. 2, from bottom to top							
D10	grey	22	25	1.1	100% He	2.65	12×300 s	8×0.05 mm^2	2 mm
D11	dark grey	22	25	1.1	20% Ne in He	3.00	12×300 s	8×0.05 mm^2	2 mm
D12	light blue	22	25	1.1	20% Ar in He	4.20	12×300 s	8×0.05 mm^2	2 mm

	Upper part IR spectra from ref. 1, from bottom to top			
trace	concentration	p_s/bar	carrier gas	scans
upper	0.16%	0.5	Ar	99
lower	0.08%	2.0	He	<150

Tab. S II. Measurement conditions for spectra depicted in fig. S 3. The count rate denoted in fig. S 3 refers to spectra #D4 and #D9.

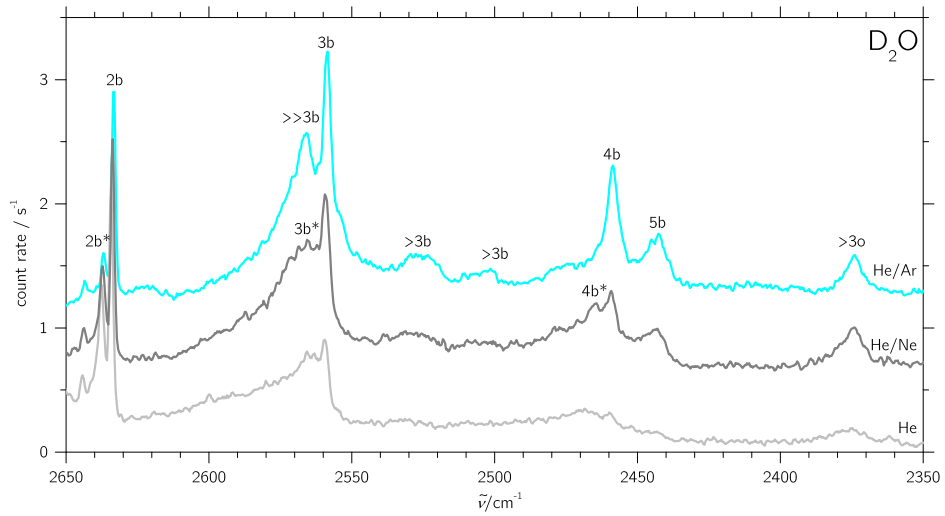

Fig. S 4. Magnified version of spectra #D10−#D12 from fig. S 3 and tab. SII. A heavier carrier gas leads to better relaxation and also to increased average cluster size.

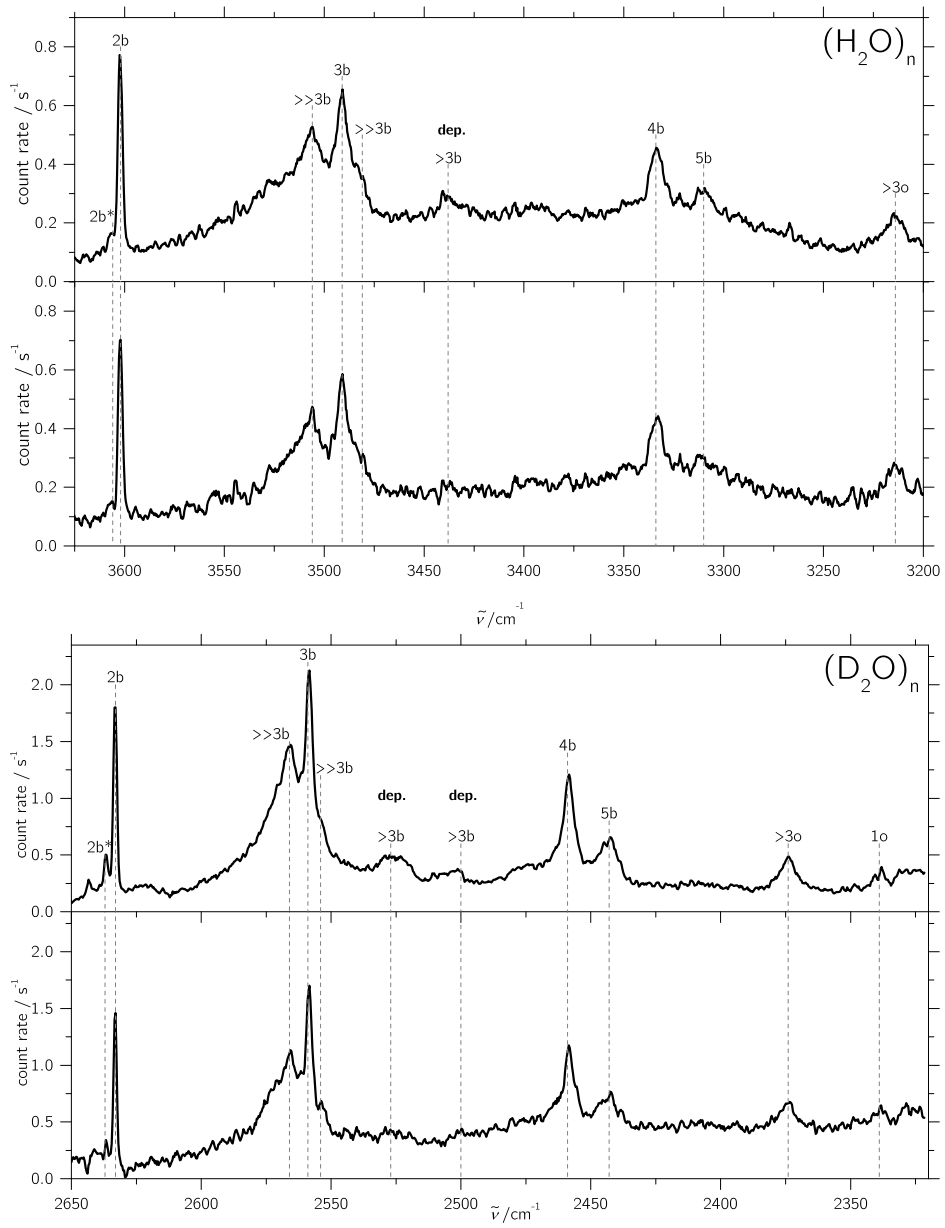

Fig. S 5. Depolarization analysis of H_2O/D_2O clusters in the OH/D stretching region. Excitation laser polarized perpendicular to the scattering plane (top trace) and residual after subtracting 7/6 of the spectrum obtained with the excitation laser polarized parallel to the scattering plane (bottom trace). All spectra were recorded under the following conditions: $\vartheta_s = 22°C$, (1.7% H_2O/D_2O in He/Ar $\approx$ 5:1), $p_s = 1.1$ bar, acquisition time 12×300 s. It is seen that only the cluster bands marked >3b are strongly depolarized.

TEMPERATURE ANALYSIS BASED ON STOKES/ANTI-STOKES TRANSITIONS

Because the detection is based on photon counting, the intensity (count) ratio is related to the temperature T and the transition wavenumber $\tilde{\nu}_\mathrm{k}$ via equation 1. $\tilde{\nu}_0$ is the excitation laser wavenumber, h Planck's constant, c the speed of light and k Boltzmann's constant.

$$\frac{I_\mathrm{Stokes}}{I_\mathrm{anti-Stokes}} = \frac{(\tilde{\nu}_0 - \tilde{\nu}_\mathrm{k})^3}{(\tilde{\nu}_0 + \tilde{\nu}_\mathrm{k})^3} \cdot \exp\left(\frac{hc\tilde{\nu}_\mathrm{k}}{kT}\right) \tag{1}$$

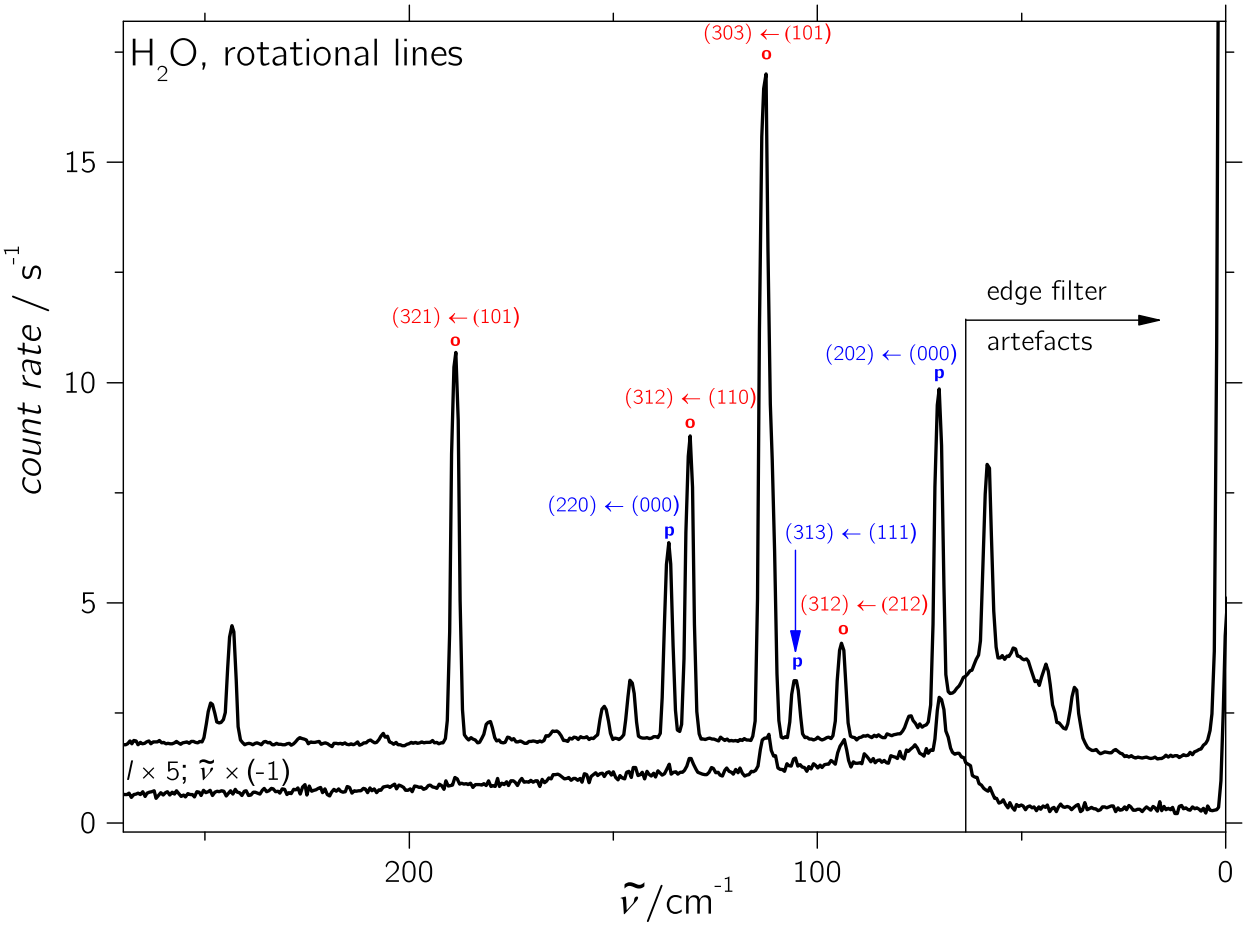

Fig. S 6. Stokes (upper) and anti-Stokes (lower) spectra of He/water expansions. $4 \times 0.15\,\mathrm{mm}^2$ nozzle at 2 mm distance and $\vartheta_\mathrm{n} = 120°\mathrm{C}$. Stagnation pressure of $p_\mathrm{s} = 0.7$ bar and saturator temperature $\vartheta_\mathrm{s} = 10°\mathrm{C}$. Acquisition time: 18×100 s (Stokes) and 36×100 s (anti-Stokes).

$\widetilde{\nu}/\mathrm{cm}^{-1}$	$I_{\mathrm{anti-Stokes}}$	I_{Stokes}	Transition	$\vartheta_{\mathrm{n}}/^{\circ}\mathrm{C}$	$T_{\mathrm{rot}}/\mathrm{K}$
70	0.642	18.726	(202) ← (000)	25	30
	0.793	15.637		25	34
	0.625	18.858		25	29
	1.557	17.641		80	41
	0.966	13.155		120	38
94	0.291	4.819	(312) ← (212)	25	48
	0.312	5.788		25	46
	0.240	4.972		25	45
	0.743	6.275		80	51
	0.336	4.565		120	63
105	0.130	3.417	(313) ← (111)	25	30
	0.063	3.172		25	38
	0.164	3.214		25	50
	0.097	3.545		80	42
	0.191	2.644		120	56
113	0.772	47.588	(303) ← (101)	25	39
	0.845	44.774		25	41
	0.537	45.944		25	36
	1.486	52.021		80	45
	0.715	38.871		120	40
131	0.234	15.375	(312) ← (110)	25	45
	0.230	15.022		25	45
	0.131	14.332		25	40
	0.403	17.748		80	49
	0.202	12.596		120	45
136	0.064	8.537	(220) ← (000)	25	40
	0.113	10.926		25	42
	0.032	10.562		25	34
	0.229	12.480		80	48
	0.121	8.264		120	45
189	0.113	18.998	(321) ← (101)	25	52
	0.100	19.034		25	51
	0.046	18.776		25	45
	0.248	26.292		80	57
	0.166	16.660		120	58

Tab. S III. Wavenumber $\widetilde{\nu}$, relative line intensities I, rotational (J K_{a} K_{c}) transition quantum numbers, nozzle temperatures ϑ_{n} in °C and effective rotational temperatures T_{rot} in K in the two-level system according to equation 1. The three results for ϑ_{n}=25 °C are three independent measurements.

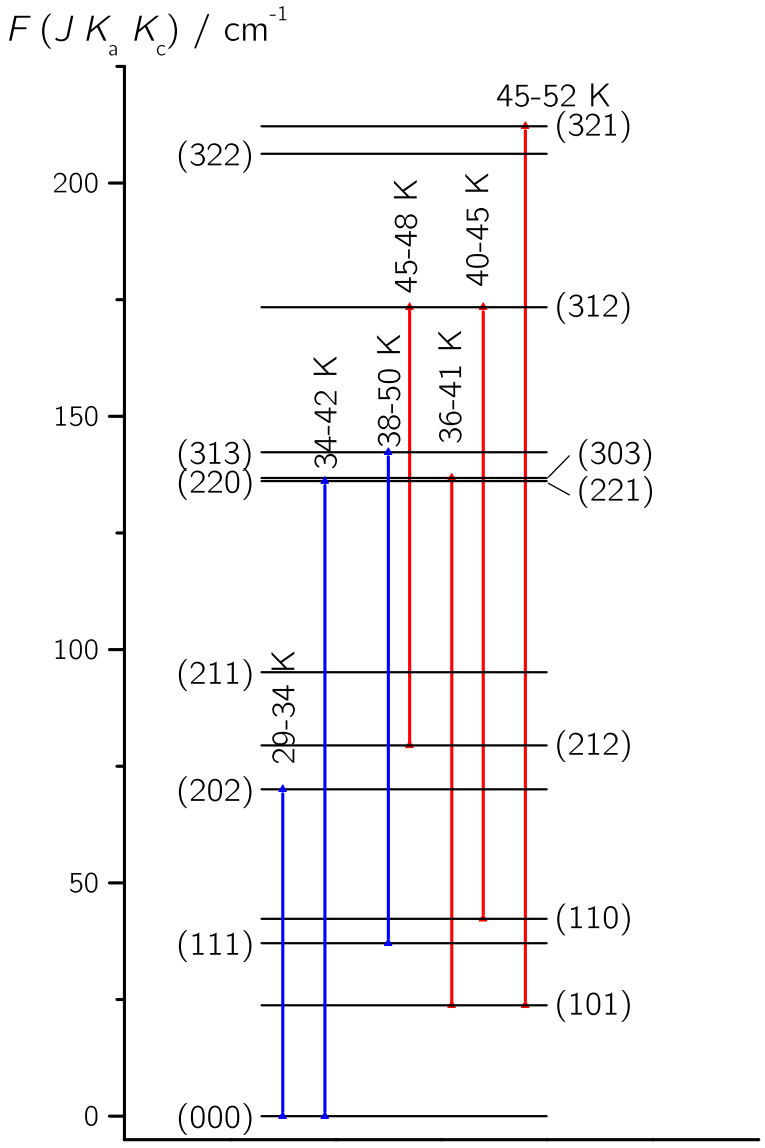

Fig. S 7. Temperature range found for pairs of water rotational levels connected by Raman transitions for a nozzle temperature of ϑ_n=25 °C and expansion in He. The rotational levels are characterized by J, K_a and K_c quantum numbers in this sequence. Labels on the left correspond to para-H_2O, labels on the right to ortho-H_2O. The para transitions are marked by blue arrows and the ortho transitions by red arrows.

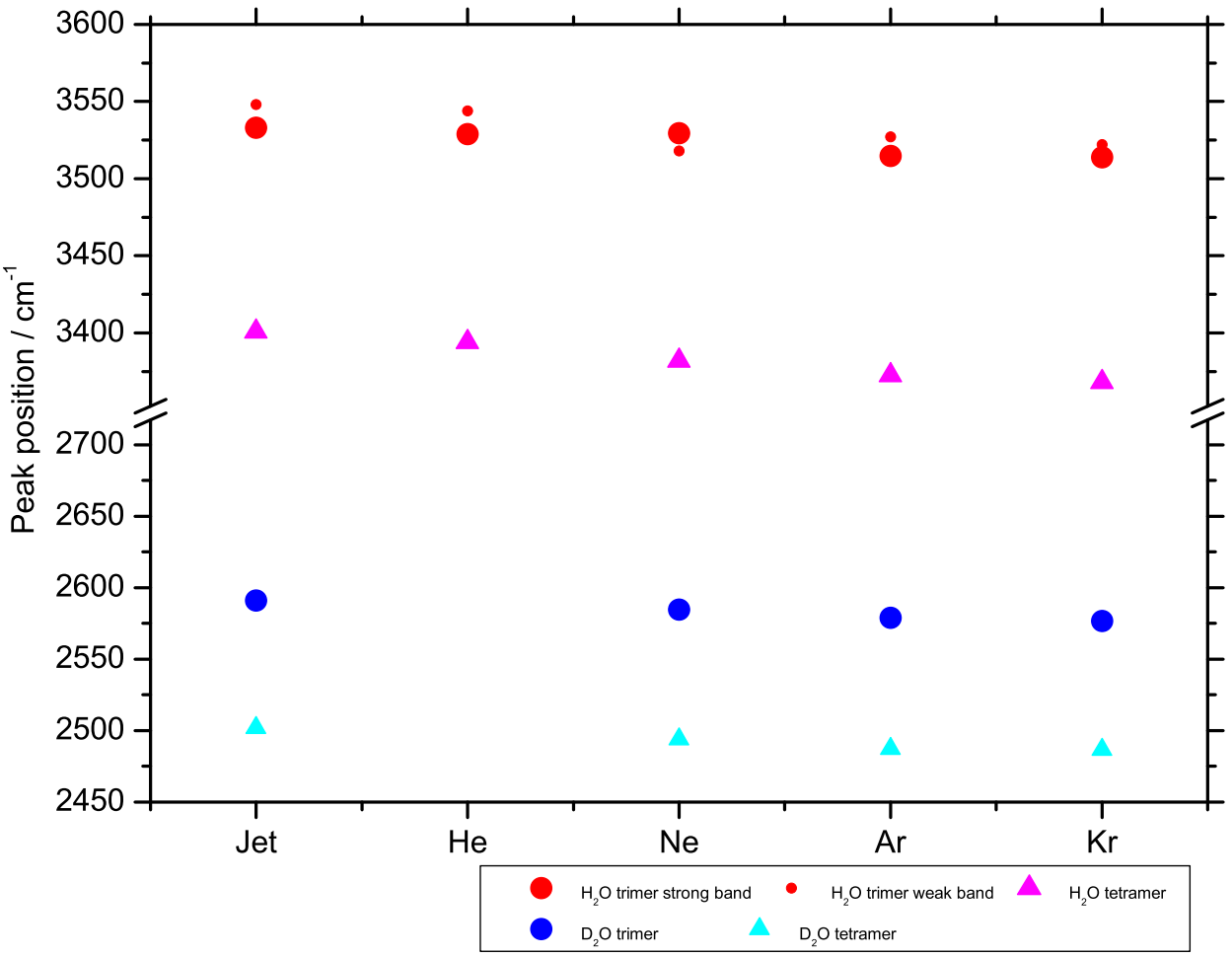

Fig. S 8. Peak positions of the IR trimer and tetramer bands for different environments. Going from gas phase[1] via He-droplets[3], Ne- and Ar-matrices to Kr-matrix[4] environment, the peak positions linearly shift to the red for trimer and tetramer and for both H_2O and D_2O. It is noteworthy that the shoulder found for the H_2O trimer is usually situated on the high frequency side of the strong band except in the neon matrix.

Method	Variant	Electronic structure	W_1/cm^{-1}	W_2/cm^{-1}	$(W_1+W_2)/\mathrm{cm}^{-1}$
Harmonic[5]		RWK2-H	25	5	29
Harmonic[6]		HF/6–31G*	22	8	31
Harmonic[7]		MP2/aug-cc-pVDZ	33	14	47
Harmonic[8]	scaled	B3LYP/6–311++G(d,p)	25	11	37
Harmonic[9]		B3LYP/d-aug-cc-pVTZ	32	13	45
Harmonic[10]	BSSE-corrected	MP2/6–311+G(2d,2p)	25	10	35
Vibrational CI[10]	BSSE-corrected	MP2/6–311+G(2d,2p)	21	11	32
Vibrational CI[10]	with BSSE	MP2/6–311+G(2d,2p)	52	30	82
Harmonic[11]		CCSD(T)/aug-cc-pVDZ	28	12	40
Harmonic[11]		LCCSD(T)/aug-cc-pVDZ	20	7	26
Harmonic[11]		LCCSD(T)/aug-cc-pVTZ	23	9	32
Harmonic[11]	no 4-body terms	PES(1,2,3)	13	5	18
Harmonic[12]		B1LYP/aug-cc-pVTZ	32	14	46
Harmonic[12]		B1LYP/cc-pVTZ	37	16	53
VPT2[12]		B1LYP/cc-pVTZ	44	28	72
P_VMWCI$_2$[12]		B1LYP/cc-pVTZ	35	20	55
Harmonic[13]	Full-dimensional	WHBB-surface	13	1	13
Harmonic[13]	LMon-β_{full}	WHBB-surface	13	0	13
Anharmonic[13]	LMon-β_{full}	WHBB-surface	12	0	12
Anharmonic[14]	MP2 VPT2 est.	CCSD(T)/aug-cc-pVDZ	21	7	28
Experiment H_2O	IR + Raman	non-Born-Oppenheimer	26	8	34
Experiment D_2O	IR + Raman	non-Born-Oppenheimer	17	5	22
Experiment CH_3OH[15]	IR + Raman	non-Born-Oppenheimer	29	11	40
Experiment CH_3OD[15]	IR + Raman	non-Born-Oppenheimer	23	≈ 8	≈ 31

Tab. S IV. Extended version of table 2. Different theoretical results for the nearest neighbor (W_1) and distant (W_2) coupling parameters of the hydrogen-bonded OH stretching manifold of water tetramer compared to the present experimental results for $(H_2O)_4$ and $(D_2O)_4$ as well as the more strongly bound "methylated" water tetramers [15]. The tabulated sum W_1+W_2 is particularly robust from the experimental point of view.

Method	Variant	Electronic structure	W/cm^{-1}	W_1/cm^{-1}	W_2/cm^{-1}
Harmonic[5]		RWK2-H	35	53	12
Harmonic[6]		HF/6–31G*	15	16	13
Harmonic[7]		MP2/aug-cc-pVDZ	21	23	17
Harmonic[16]		CCSD/DZP+diff	25	26	21
Harmonic[17]		MP2/TZP	21	23	17
ccVSCF[17]		MP2/TZP	53	60	39
Harmonic[18]		MP2/aug-cc-pVTZ	23	25	18
Harmonic[18]		MP2/TZ2P(f,d)+dif	22	25	17
Harmonic[18]		B3LYP/TZ2P(f,d)+dif	22	25	17
Harmonic[18]		B3PW91/TZ2P(f,d)+dif	25	28	19
Harmonic[8]	scaled	B3LYP/6–311++G(d,p)	16	18	12
Anharmonic[8]		B3LYP/6–311++G(d,p)	17	20	12
Harmonic[19]	scaled	MP2/aug-cc-pVTZ	22	24	18
Anharmonic[19]		MP2/aug-cc-pVTZ	18	20	12
Harmonic[9]	scaled	B3LYP/d-aug-cc-pVTZ	21	23	17
Harmonic[10]	BSSE-corrected	MP2/6–311+G(2d,2p)	17	19	13
Vibrational CI[10]	BSSE-corrected	MP2/6–311+G(2d,2p)	19	21	16
Vibrational CI[10]	with BSSE	MP2/6–311+G(2d,2p)	24	26	20
Harmonic[20]	Table II	PES(ACPF/cc-pVTZ)	16	18	12
Harmonic[20]	Table IV	PES(ACPF/cc-pVTZ)	8	14	7
Vibrational CI[20]		PES(ACPF/cc-pVTZ)	25	28	20
Harmonic[11]		PES(1,2,3)	11	13	7
Harmonic[11]		CCSD(T)/aug-cc-pVTZ	20	22	16
Harmonic[11]		CP-CCSD(T)/aug-cc-pVTZ	18	20	14
Harmonic[11]		LCCSD(T)/aug-cc-pVTZ	15	16	11
Harmonic[12]		B1LYP/cc-pVTZ	26	27	23
Harmonic[12]		B1LYP/aug-cc-pVTZ	21	23	16
Harmonic[12]		B3LYP/cc-pVTZ	28	29	25
Harmonic[12]		MP2/cc-pVTZ	28	29	25
VPT2[12]		B1LYP/cc-pVTZ	20	21	17
P_VMWCI$_2$[12]		B1LYP/cc-pVTZ	32	34	27
Harmonic[21]		LCCSD(T)/aug-cc-pVQZ	21	23	17
Harmonic[21]	3b5 fit	WHBB-surface	8	10	4
Harmonic[21]	3b6 fit	WHBB-surface	15	17	10
Harmonic[14]		CCSD(T)/aug-cc-pVDZ	18	20	15
Anharmonic[14]	MP2 VPT2	CCSD(T) est./aug-cc-pVDZ	15	17	9
Experiment H_2O (3_A)	IR+Raman	non-Born-Oppenheimer	14	14	14
Experiment H_2O (3_B)	IR+Raman	non-Born-Oppenheimer	17	20	9
Experiment D_2O	IR+Raman	non-Born-Oppenheimer	11		
Experiment CH_3OH[15]	IR+Raman	non-Born-Oppenheimer	20	21	17
Experiment CH_3OD[15]	IR+Raman	non-Born-Oppenheimer	13	14	11

Tab. S V. Extended version of table 3. Different theoretical values for the coupling constant W for a C_3-symmetric trimer (simple Hückel model, one level with A-symmetry (Raman active) and two degenerate levels of E-symmetry (IR-active)) and coupling constants W_1 and W_2 for the more complex case where the three hydrogen bonds differ in strength (asymmetric coupling). Experimental trimer coupling constants are less certain than tetramer constants because of the reduced symmetry, the potentially large tunneling splitting, and the intensity difference of the two observed IR-active bands.

Method	Variant	Electronic structure	W_1/cm^{-1}	W_2/cm^{-1}	$W_1+\frac{\sqrt{5}+1}{\sqrt{5}-1}\cdot W_2/\mathrm{cm}^{-1}$
Harmonic[22]		MP2/aug-cc-pVDZ	35	9	58
Harmonic[8]	scaled	B3LYP/6–311++G(d,p)	27	9	50
Anharmonic[8]		B3LYP/6–311++G(d,p)	36	26	104
Harmonic[19]	scaled	HF/6–31G*	20	5	34
Harmonic[9]	scaled	B3LYP/d-aug-cc-pVDZ	34	10	60
Harmonic[10]	BSSE-corrected	MP2/6–311+G(2d,2p)	26	7	45
Vibrational CI[10]	BSSE-corrected	MP2/6–311+G(2d,2p)	26	6	42
Vibrational CI[10]	with BSSE	MP2/6–311+G(2d,2p)	43	34	133
Harmonic[13]	Full-dimensional	WHBB-surface	14	-0.3	13
Harmonic[13]	LMon-β_{dimer}	WHBB-surface	14	-0.2	14
Anharmonic[13]	LMon-β_{dimer}	WHBB-surface	15	-0.2	14
Harmonic[14]		CCSD(T)/aug-cc-pVDZ	30	9	53
Anharmonic[14]	MP2 VPT2 est.	CCSD(T)/aug-cc-pVDZ	36	21	90
Experiment H_2O	IR + Raman	non-Born-Oppenheimer	–	–	33
Harmonic[22] D_2O		MP2/aug-cc-pVDZ	24	8	44
Experiment D_2O	IR + Raman	non-Born-Oppenheimer	14	4	25

Tab. S VI. Extended version of table 4. Different theoretical results for the nearest neighbor (W_1) and distant (W_2) coupling parameters for the simple model of a C_{5h} symmetric water pentamer. Since the minimum structure of the pentamer is not C_{5h} symmetric and therefore exhibits no degeneracies, the mean values of the two IR active (corresponding to E'$_1$) and the highest lying two Raman active (corresponding to E'$_2$) bands have been used for the calculation of the coupling constants. The combination $W_1+\frac{\sqrt{5}+1}{\sqrt{5}-1}\cdot W_2$ in the last column does not depend on the uncertain assignment of the weakly Raman active transition and is therefore most reliable.

SUPPLEMENTARY REFERENCES

[1] D. J. Nesbitt, T. Häber, and M. A. Suhm, Faraday Discuss. **118**, 305 (2001).

[2] Z. Xue, Ph.D. thesis, Universität Göttingen (2010).

[3] C. J. Burnham, S. S. Xantheas, M. A. Miller, B. E. Applegate, and R. E. Miller, J. Chem. Phys. **117**, 1109 (2002).

[4] J. Ceponkus, G. Karlström, and B. Nelander, J. Phys. Chem. A **109**, 7859 (2005).

[5] J. R. Reimers and R. O. Watts, Chem. Phys. **85**, 83 (1984).

[6] E. Honegger and S. Leutwyler, J. Chem. Phys. **88**, 2582 (1988).

[7] S. S. Xantheas and T. H. Dunning, J. Chem. Phys. **99**, 8774 (1993).

[8] K. Ohno, M. Okimura, N. Akai, and Y. Katsumoto, Phys. Chem. Chem. Phys. **7**, 3005 (2005).

[9] H. Cybulski and J. Sadlej, Chem. Phys. **342**, 163 (2007).

[10] Y. Watanabe, S. Maeda, and K. Ohno, J. Chem. Phys. **129**, 074315 (2008).

[11] Y. Wang, B. C. Shepler, B. J. Braams, and J. M. Bowman, J. Chem. Phys. **131**, 054511 (2009).

[12] D. Bégué, I. Baraille, P. A. Garrain, A. Dargelos, and T. Tassaing, J. Chem. Phys. **133**, 034102 (2010).

[13] Y. Wang and J. M. Bowman, J. Chem. Phys. **136**, 144113 (2012).

[14] E. Miliordos, E. Aprà, and S. S. Xantheas, J. Chem. Phys. **139**, 114302 (2013).

[15] R. W. Larsen, P. Zielke, and M. A. Suhm, J. Chem. Phys. **126**, 194307 (2007).

[16] J. E. Fowler and H. F. Schaefer III, J. Am. Chem. Soc. **117**, 446 (1995).

[17] G. M. Chaban, J. O. Jung, and R. B. Gerber, J. Phys. Chem. A **104**, 2772 (2000).

[18] J. A. Anderson, K. Crager, L. Fedoroff, and G. S. Tschumper, J. Chem. Phys. **121**, 11023 (2004).

[19] M. E. Dunn, T. M. Evans, K. N. Kirschner, and G. C. Shields, J. Phys. Chem. A **110**, 303 (2006).

[20] Y. Wang, S. Carter, B. J. Braams, and J. M. Bowman, J. Chem. Phys. **128**, 071101 (2008).

[21] Y. Wang, X. Huang, B. C. Shepler, B. Braams, and J. M. Bowman, J. Chem. Phys. **134**, 094509 (2011).

[22] S. Graf, W. Mohr, and S. Leutwyler, J. Chem. Phys. **110**, 7893 (1999).